Computers & Fluids 39 (2010) 1275–1283

Contents lists available at ScienceDirect

Computers & Fluids

journal homepage: www.elsevier.com/locate/compfluid

Modeling of indoor airflow and dispersion of aerosols using immersed boundary and random flow generation methods

Shaolin Mao *, Ismail B. Celik

Mechanical and Aerospace Engineering Department, West Virginia University, Morgantown, WV 26506-6106, USA

ARTICLE INFO

Article history:
Received 9 March 2009
Received in revised form 19 February 2010
Accepted 26 March 2010
Available online 1 April 2010

Keywords:
Aerosol dispersion
Lagrangian stochastics
Indoor air
Random flow generation
Finite volume method
Immersed boundary method

ABSTRACT

Numerical modeling of environmental flows involves complex geometry, moving bodies, multi-phase flow, and buoyant jet effects. An in-house CFD code has been developed using finite volume and immersed boundary methods. The transport and dispersion of virus-laden aerosols in a ventilated room is investigated by this numerical code. The uniqueness of this numerical code is that it can efficiently compute small-scale turbulent flow in which most commercial CFD software will suffer from large numerical error. Random flow generation (RFG) [33] is an ideal choice for small-scale turbulence for low-Reynolds number flow in a ventilated room. In addition, Lagrangian stochastic (LS) walk model is applied to directly compute probability density function (PDF) of aerosols and estimate the risk factor of aerosol dispersion from a point source. The present study focuses on aerosols with small diameter (<10 μm) in which the effects of evaporation on the dispersion of aerosols could be neglected. Different location of aerosol sources and a typical ventilation layout are discussed in detail. The numerical results with PDF yield more useful quantitative information to assess the risk area of virus transport in a ventilated room than that shown in random trajectories of particles as widely reported in the literature. This study provides valuable information for ventilation control strategies with respiratory protection, such as enhanced air exchange, air filtration rate, and improved airflow patterns to reduce indoor infection risk via airborne virus laden droplets.

1. Introduction

Airborne transmission of diseases like influenza is of great concern to the public health community. Bio-aerosols have been referred as an important mode of transmission of influenza by many researchers [36], and references therein [2,3,24,28]. The virus-containing bio-aerosols originate from the respiratory activities such as coughing and sneezing. For instance, influenza viruses are believed to spread through the air via turbulent diffusion and transport and infect others who walk in. Modeling of the dispersion of respiratory virus-laden aerosols in a ventilated room is a viable approach to examine the safety and reliability of engineering control measures. Mathematical modeling can provide detailed three-dimensional information of infectious aerosol transmission at a given time which is hard to directly obtain from experimental observation or sampling.

Several analytic or semi-analytic models have been proposed to evaluate risk factors for airborne transmission of diseases [6,11,22,23,30,39,40]. However, these models suffer from neglecting the effects of fine scale turbulence on the spatial and temporal distribution of bio-aerosols. In the past decade, most work on modeling of indoor airflow and airborne transmission of aerosols or droplets rely on computational fluid dynamics (CFD) models. For example, indoor air quality, thermal comfort, and distribution of indoor contaminant particles have been well documented by using CFD tools [7,8,15,19,35]. The majority of these studies have dealt with averaged turbulent flow and scalar fields by using Reynolds averaged Navier–Stokes (RANS) turbulent transport models. Qualitative estimation of trajectories of single or group particles rather than direct estimation of most risk areas has been reported. Shih et al. [31] investigated the effect of moving body in a ventilated room using dynamic meshes. Tian et al. [38] showed instantaneous re-circulation structure in velocity field in a ventilated room using large-eddy simulation (LES). However, a challenging task is to simulate small-scale turbulence or intermittency of turbulence, for example buoyant jets (coughing or sneezing) in an isolated room. Specific low-Reynolds number turbulent transport models are required for the prediction of low-velocity indoor airflows which is not suitable by using commercial CFD software such as FLUENT on relatively coarse grids. Furthermore, it is much more difficult to predict second-order moments such as Reynolds stresses and auto-variances. Improvement can be sought by using an alternative

* Corresponding author. Present address: Advanced Dynamics Inc, Lexington, KY 40511, USA.
E-mail address: slm_wvu@yahoo.com (S. Mao).

0045-7930/$ - see front matter © 2010 Elsevier Ltd. All rights reserved.
doi:10.1016/j.compfluid.2010.03.010

numerical technique such as random flow generation (RFG) technique to reconstruct fine scale turbulence from the mean quantities already calculated [33].

The above fluid dynamics problems usually involve complex geometries and moving boundaries in addition to strong transients. The applications of CFD to such problems traditionally employ boundary fitted coordinates, which require generation of complicated computational grids. The alternative approach utilizing Cartesian coordinates with embedded virtual force method (immersed boundary method) avoids the problem of expensive and time consuming boundary fitted grid. The simple rectangular or hexahedral orthogonal grids directly benefit numerical accuracy and computational efficiency. An immediate application of immersed boundary method [26,34] is to modify an in-house CFD DREAM code [1,4,13,14]. The available DREAM code was developed by the CFD & AMP Center (http://cfd.mae.wvu.edu) at the Department of Mechanical and Aerospace Engineering, West Virginia University, WV, USA.

The objective of the present study is to develop a novel CFD tool for bio-fluids and environmental flow applications such as gas-droplets multi-phase flow simulation, in particular, droplets and particles dispersion and migration in air-conditioning environment, risk assessment of biological aerosols and virus-laden particles in workplaces. For the purpose of computational efficiency, a simple and orthogonal Cartesian grid has been used thanks to benefits of the immersed boundary method. The so-called unsteady RANS model is used without directly using a wall function for turbulent flow. By employing the random flow generation (RFG) [33] technique, small-scale homogeneous or inhomogeneous turbulent fluctuations are captured without complicated turbulence models. In addition, the code is linked to a Lagrangian stochastic (LS) model [10] to compute probability density function (PDF) of small-size droplets migration in a ventilated room. The LS model has several advantages such as direct tracking of fluid particle trajectories, meshless, independence of the reference frame, without numerical diffusion, concentration is always positive, and feasibility in conjunction with complicated flow environment. A static circular cylinder in uniform flow field is used to benchmark the DREAM code. A typical ventilation system is applied, and different locations of aerosol sources to mimic standing, sitting, or sleeping position of a subject are discussed in detail. A simple cough model with constant temperature and constant relative humidity is assumed. The simulation is limited to small aerosols (with diameter <10 μm) which are diluted enough that its effects on the continuous phase, air, can be neglected.

2. Mathematical model

The physical properties of aerosols are strongly dependent on droplets or particles size. Aerosols with an aerodynamic diameter (<10 μm) remain suspended in air for a sufficient duration to permit dispersion through the room [36]. Large aerosols or droplets (>10 μm) are characterized by evaporation and settling in the room. The evaporation process affects the drifting velocity of droplets and its concentration [9,12]. Numerical experiments showed that the evaporation process of 50 μm droplets finished in several seconds as their diameter reduced to less than 5 μm under the condition of 60% relative humidity [20]. Experiments showed that 90% of large size (d > 50 μm) water droplets rapidly settle down close to point of emission, only about 4–10% of droplets disperse in room air (d < 10 μm), and the time-scale for the process of evaporation of droplets from 5–10 μm to 2 μm is less than 0.1 s [21]. Considering 1.0 m/s air velocity in the room, the maximum distance for droplets with large size to settle down is about 0.1 m for 99% particles involved. Size distribution experiment also shows that 82% of droplet nuclei is in range of 0.74–2.12 μm, and which are possible key contributors to airborne disease transmission [41]. The dispersion of these suspended droplets with small size is the main focus of this study. It is reasonable to assume that the dispersion and transport of aerosols can be regarded as passive scalars (i.e. all particles follow the air in perfect harmony). Thus, the dispersion of passive scalar (influenza virus) by turbulent fluctuations can be considered as an archetypal continuous stochastic process. Numerical simulation shows that it is justified to model these aerosols as passive scalars, which neutrally follow the turbulent airflow, as a first approximation.

2.1. Modeling of continuous phase flow by finite volume method

Indoor airflow is characterized as a low-Reynolds number turbulent flow. The air–aerosols dynamics is determined by a one-way coupling process. The carrier phase (air) solution is independent of the particle trajectories assuming that the particulate phase is diluted and does not affect the carrier phase. The continuous phase airflow in an isolated room is modeled by so-called unsteady RANS with no turbulence model (URANS) where random flow generation (RFG) (see Section 2.2) is used to generate small-scale turbulence. The large-scale turbulent flow (not the mean velocity) is obtained by solving the following governing equations:

$$\begin{aligned}
&\frac{\partial u_i}{\partial x_i} = 0 \\
&\frac{\partial u_i}{\partial t} + \frac{\partial u_i u_j}{\partial x_i} = -\frac{\partial p}{\partial x_i} + \nu \frac{\partial^2 u_i}{\partial x_i \partial x_j} - \frac{\partial \tau_{ij}}{\partial x_j} \\
&\frac{\partial T}{\partial t} + \frac{\partial T u_j}{\partial x_j} = \kappa \frac{\partial^2 T}{\partial x_i \partial x_j} - \frac{\partial T_{\theta j}}{\partial x_j} \\
&\frac{\partial C}{\partial t} + \frac{\partial (C u_j)}{\partial x_j} = \frac{\partial}{\partial x_j}(D_1 + D_2)\frac{\partial C}{\partial x_j} + S_c
\end{aligned} \tag{1}$$

where τ_{ij} and $\tau_{\theta j}$ are the small scale Reynolds stresses and scalar fluxes, respectively. The diffusion coefficient in the concentration equation contains two terms, one for molecular effect and another for turbulent transport modeled via an RFG technique. The differential conservative form of Eq. (1) is given by

$$\frac{\partial}{\partial t}(\rho\phi) + \frac{\partial}{\partial x_j}(\rho u_j \phi) = \frac{\partial}{\partial x_j}(\Gamma \frac{\partial \phi}{\partial x_j}) + S_\phi \tag{2}$$

Standard finite volume method is applied to discretize Eqs. (1) or (2) by using structured orthogonal and staggered grid for velocities, temperature and pressure [25]. The discrete form of Eq. (2) can be written as follows [1,4,13]:

$$a_P \phi_P = \sum a_{nb} \phi_{nb} + b \tag{3}$$

where a_x are the coefficients of the corresponding nodal variables, subscript "nb" denotes neighboring nodes, b is a function of ϕ evaluated at an old time level. The choices to solve the available algebraic equations are alternative direction implicit (ADI) or strongly implicit procedure (SIP, an implicit LU decomposition method).

2.2. Random flow generation (RFG) for small-scale fluctuation

The random flow generation (RFG) technique is applied in the DREAM code to construct small-scale turbulent fluctuations [33]. This model is a modified version of 16 method and can serve as a sub-grid scale (SGS) model for large-eddy simulations (LES). By choosing appropriate turbulence length-scale and time-scale, it is shown via numerical studies that RFG can achieve a flow field that resembles the flow structure simulated directly using LES [32]. Fortunately, the turbulence length-scale and time-scale can be estimated for ventilated rooms through defined geometry and

turbulence intensity. The turbulent fluctuation obtained via RFG is superimposed to the large-scale turbulent field obtained by URANS.

In order to apply RFG technique, the length-scale and time-scale in indoor airflow condition needs to be known. The mixing length-scale model is used as follows:

$$\tau = \frac{\ell}{u} \tag{4}$$

where u, the velocity scale for indoor turbulent flow, is determined from a prescribed turbulent intensity, for instance 5%. The general form of the length-scale equation is given by:

$$\{\ell = c\min\{\kappa_1\ell_x, \kappa_2\ell_y, \kappa_3 ell_z, \lambda_1 H, \lambda_2 W, \lambda_3 L, \Delta x, \Delta y, \Delta z\} \tag{5}$$

where c is chosen to be a constant (in the order of 1.0) or a function of turbulent kinetic energy, $\lambda_1 = \lambda_2 = \lambda_3 =$0.1–0.5, $\kappa_1 = \kappa_2 = \kappa_3 =$ 0.05, H, W, L are the dimensions of the room, Δx, Δy, Δz are the grid sizes, and ℓ_x, ℓ_y, ℓ_z are the distances of the point in consideration from the walls (Fig. 1). Therefore, the suggested length and time-scales are 0.04 m and 0.01 s, respectively, for this study. There are guidelines on the selection of constant lambda and kappa, first is the assumption of isotropic turbulence which results in equal values in three directions, second is three sets of geometry in our study in (5). Finally, the value of lambda and kappa are not universal and relies on experimental results. More details can be found in Tennekes and Lumley [37].

The small-scale turbulent fluctuation is generated as follows:

$$v_i(\vec{x}, t) = \sqrt{\frac{2}{N}}\sum_{n=1}^{N}\left[p_i^n \cos(\tilde{k}_j^n \tilde{x}_j + \omega_n \tilde{t}) + q_i^n \sin(\tilde{k}_j^n \tilde{x}_j + \omega_n \tilde{t})\right] \tag{6}$$

$$\tilde{x}_j = \frac{x_j}{\ell}, \quad \tilde{t} = \frac{t}{\tau}, v' = \frac{\ell}{\tau}, \quad \tilde{k}_j^n = k_j^n \frac{v'}{v'_{(j)}} \tag{7}$$

$$\begin{aligned} &p_i^n = \varepsilon_{ijm}\varsigma_j^{(n)} k_m^{(n)}, \quad q_i^n = \varepsilon_{ijm}\xi_j^{(n)} k_m^{(n)} \\ &\varsigma_i^n, \xi_i^n, \quad \omega_n \in N(0,1), \quad k_i^n \in N(0, \frac{1}{2}) \end{aligned} \tag{8}$$

where $N(M, \sigma)$ is a normal distribution with mean M and a standard deviation σ. Repeated indices imply Einstein summation, parentheses between index preclude summation. The number N in Eq. (6) is the size of spectral space.

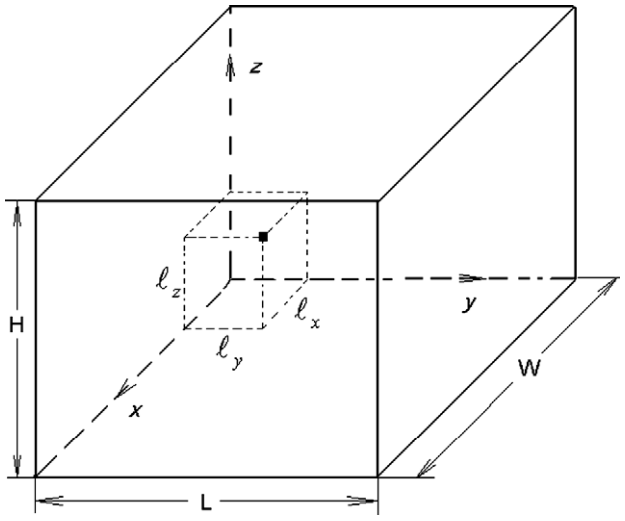

Fig. 1. Geometry for the determination of the length-scale and time-scale for indoor low-Reynolds number turbulent flow.

2.3. Immersed boundary method

For the cases where immersed boundary represents a solid surface, additional forces are added to the governing equations to represent the surface [26]. Traditionally, immersed boundary method has been used for two-way coupling virtual forces. Since the immersed boundary method is used for stationary subjects such as mannequin, or desk/chairs in test room, the process of calculation of virtual force can be simplified in this study. The forcing concept is based on a one-way coupling between the solid and fluid, i.e., the solid influences the fluid, but the fluid does not influence the solid body. Fig. 2 shows the calculation of u_i in the computational cell (gray cell) most close to the body surface where the value of u_i is required to calculate the virtual force [34]. Without loss of generality, the momentum equations in (1) are recast

$$\frac{u^{l+1} - u^l}{\Delta t} = RHS^{l+\frac{1}{2}} + f^{l+\frac{1}{2}} \tag{9}$$

where superscript "ℓ" imply current time level, and "$\ell + 1/2$" means intermediate value. The RHS contains convective, diffusive (viscous), pressure gradient, and source terms. The additional term f is introduced by the immersed boundary method. Given the value of u_i (Fig. 2), the virtual forcing term is obtained from

$$f^{l+\frac{1}{2}} = -\mathrm{RHS}^{l+\frac{1}{2}} + \frac{u_i - u^l}{\Delta t} \tag{10}$$

the above value of f is then added to the momentum equation for the calculation at next time level "$\ell + 1$". A simple way to compute the virtual force term is suggested by Su et al. [34],

$$f = -\beta v_n + \alpha v_n |v_n| \tag{11}$$

where β and α are empirical parameters. Eq. (11) is used in this study with the value of:

$$\alpha = 10, \quad \beta = \frac{0.8}{\Delta t} \tag{12}$$

There are detailed benchmark reports about this approach and it has led to very good results in a variety of test cases. This simplified approach provides globally accurate results for relatively coarse

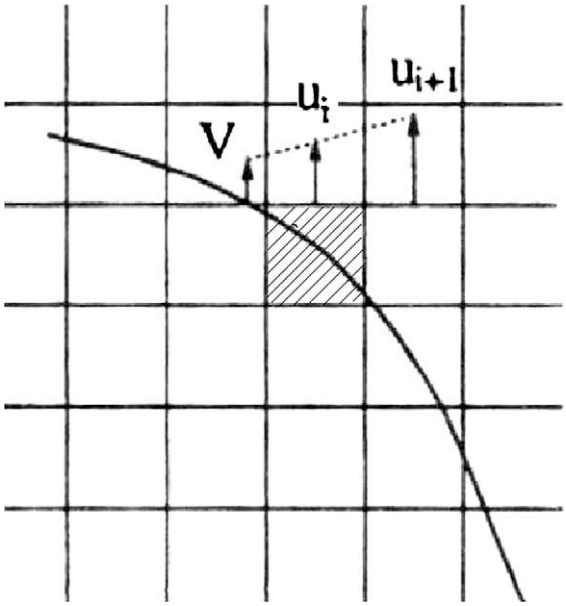

Fig. 2. Calculation of the gray cell velocity close to the surface by linear interpolation between the velocity of the body and the velocity of the adjacent fluid cell.

grids. In order to resolve the small-scale turbulent flow around solid surfaces, finer grid is usually required close to the solid surface. Advanced techniques such as dynamic adaptive mesh refinement (AMR) provide an effective solution. In the current study, instead of directly applying a wall function, the non-slip boundary on the solid surface has been implemented by using two free parameters in the immersed boundary method Eqs. (11) and (12). By a suitable selection of free parameters, the three velocity components approach zero rapidly on the solid surface on which the non-slip boundary condition satisfies. The details of the boundary layers in the immediate vicinity of the walls were not considered to be critical for droplet dispersion model (see next section). The root mean turbulent fluxes are obtained with the help of the RFG method.

2.4. Modeling of dispersion and transport of aerosols

The mathematical model of the dispersion of particles in this study is a stochastic process. The Lagrangian stochastic (LS) model (Markov-chain model) is introduced to simulate individual particle trajectory by assuming that its velocity can be represented by a Markov sequence [10]. Unlike the Eulerian–Eulerian or hybrid Eulerian–Lagrangian approach, the LS model is not dependent on mesh resolution or the number of trajectories computed. Given a turbulent flow, the problem is posed to describe statistically the evolution of the aerosol field from a known initial state. Turbulent diffusion and advection was computed in the vertical and two horizontal directions using the LS model. For instance, the vertical displacement of aerosol particles is computed as a function of time,

$$dz = w \cdot dt \tag{13}$$

where w is the Lagrangian vertical velocity fluctuation and dt is differential time increment. Incremental change in vertical velocity were computed using the Langevin equation [10], and references therein),

$$dw = a(z,t,w)dt + b(z,t,w)d\xi \tag{14}$$

where the first term in the RHS is due to a deterministic forcing (systematic forcing), and the second term describes a random forcing term [5]. The two coefficients are derived from the Fokker–Planck equation [10]. $d\xi$ defines a Gaussian distribution with a mean of zero and variance of dt. Instead of direct calculation of the coefficients $a(z,t,w)$, $b(z,t,w)$, here RFG technique is used to compute the random forcing term. It must be pointed out that the particles are small enough to suspend in the air (diameter less than 10 μm) and can be treated as passive scalar which justifies the application of Langevin equation above.

An important time-scale with LS model is the Lagrangian integral time-scale T_L. For the discrete form, when we consider the particle velocities at discrete times, $t_0, t_1, \ldots, t_n$, where $t_{n+1} - t_n = \Delta t$, the following relation should be required:

$$T_\lambda < \Delta t < T_L \tag{15}$$

where T_λ is the time-scale over which the particle acceleration remains correlated. A practical choice is,

$$\Delta t = (0.05 \approx 0.1)T_L \tag{16}$$

2.5. Boundary conditions for particulate phase

In order to represent the effects of entrainment and deposition of aerosols when they are in contact with the wall, a simple model is used as follows:

$$\dot{Q}_D^{net} = \dot{Q}_D - \dot{Q}_E = c^* \sqrt{k} \tag{17}$$

where c^* is a constant, and k is the turbulent kinetic energy. The subscript "D" and "E" denote the deposition and entrainment, respectively. It is also important to consider the non-physical wall collision by introducing a de-correlation factor in the near wall model. A threshold of the kinetic energy of a droplet in this study is used to determine whether it is "reflected" or "trapped" [18]. For simplicity, it is assumed that the indoor droplet deposition occurs mainly on the floor surface, while the deposition of droplets on the ceiling surface is weak where particle-bouncing condition is a reasonable choice.

3. Numerical results

3.1. Modeling of indoor airflow and aerosol transport

A representative type of ventilation layout is used (Fig. 3). A simple inlet and outlet vent replaces complicated diffuser in our simulation. Uniform inlet jet and steady state ventilation airflow is considered. The velocity at the inlet is assumed to be 0.4 m s^{-1}.

The location of coughing source is located at (1.125 m, 0.34 m, 1.125 m). A cough has a total content of 4000 ml and duration of 1 s analogous to an adult's cough. The typical boundary condition

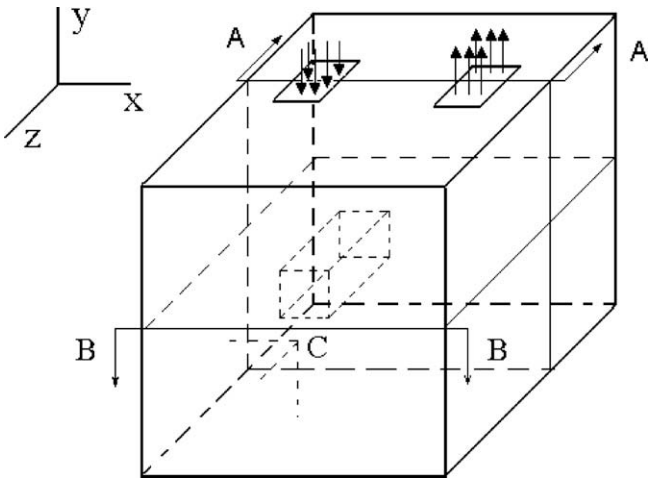

Fig. 3. Layout of inlet and outlet for a ventilation room, a vertical (A–A slice) and a horizontal (B–B slice) cross section are chosen. The diffuser area is 0.4 m × 0.2 m for inlet and outlet vent. Point C shows the position of the source.

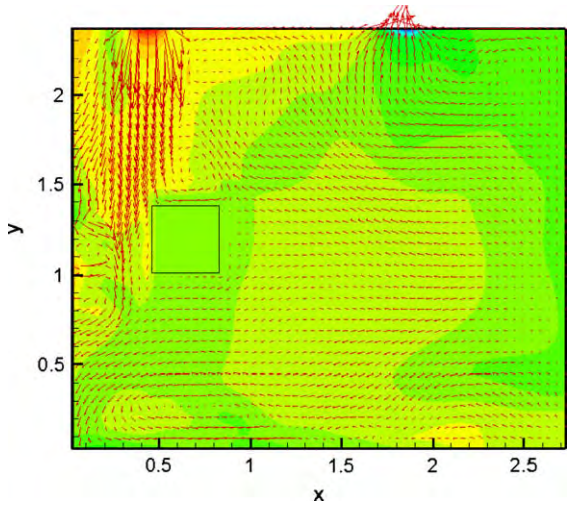

Fig. 4. Instantaneous velocity field shown at the vertical cross section (A–A slice): arrows show the $u\_$ and $v\_$ velocity components and color contours show $w\_$ velocity component. x and y in meters.

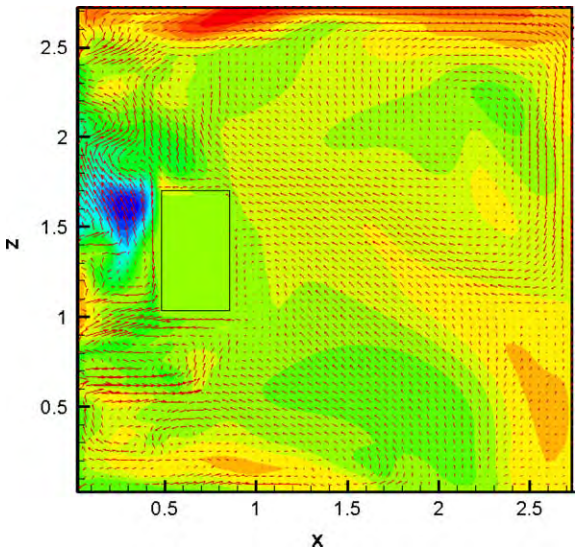

Fig. 5. Instantaneous velocity field shown at a horizontal cross section (B–B slice): arrows show u_ and w_velocity components and color contours show v_velocity component. x and y in meters.

for a coughing jet mimics an experimental condition performed at NIOSH [27]. Given the 12 l s^{-1} of flow rate, the maximum velocity from an initial axissymmetric round jet can be calculated in which the diameter of the jet nozzle is 20 mm. The initial velocity from the jet is in the x direction. The inlet concentration of aerosols is zero (background concentration), and Neumann boundary condition at the outlet is imposed for the scalar. The computational domain is 2.75 m × 2.45 m × 2.75 m. Structured Cartesian grids are used in the domain with 524,000 grid cells. A time-step of 10^{-5} s was used in fully implicit time scheme. Two cross sections are selected to show instantaneous or mean values of flow and scalar fields. Figs. 4 and 5 show an instantaneous velocity field at the vertical A–A slice and horizontal B–B slice, respectively. Strong airflow mixing is shown from the re-circulation structure in the velocity field. Fig. 6 shows time series of air instantaneous velocities at a point inside the room. It demonstrates that our URANS model combined with RFG technique has effectively captured both large-scale and small-scale turbulence. Our results demonstrate an advantage over RANS transport models in which the spatial and temporal fluctuations in the momentum and scalar field and local instantaneous exposure may not be effectively captured. The RANS-tied URANS method shows LES like capability (pseudo-LES).

Figs. 7 and 8 show instantaneous distribution of aerosol concentration at four consecutive instants with the time interval of 1 s with and without coughing jet in a closed ventilation room. A point source with unit strength is released from t = 1 s–2 s in the room to mimic an adult's cough. The initial location of the point source is at the cell (0.675 m, 0.96 m, 0.855 m). Fig. 7 shows a dominant downward advection on the transport of aerosols, which rapidly settle down to the floor. Considering the effect of coughing buoyant jet, however, the maximum value of concentration decreases and aerosols dilute rapidly after 50 s because the coughing jet enhances dispersion of aerosols as shown in Fig. 8. The difference of the highest concentration in Figs. 7 and 8 is more than two-orders of magnitude due to the effects of coughing jet. The well-mixing condition of passive scalars may be justified for cases with strong airflow or coughing jet conditions. However, because of indoor air being ventilated with fresh air at a given air change per hour (ACH), the concentration of aerosols shows large difference even though the velocity field is fully developed.

3.2. Small-scale turbulence and its effects

One application of our numerical code is modeling of small-scale turbulence and its effects on the dispersion of particles in a ventilated room. Representative examples are a turbulence driven by coughing in a room (buoyant jet), or by a blender (pure mechanical power). The feature of the flow is its zero mean velocity even though local strong turbulence happens. Most turbulent transport models cannot effectively catch the turbulence fluctuation while

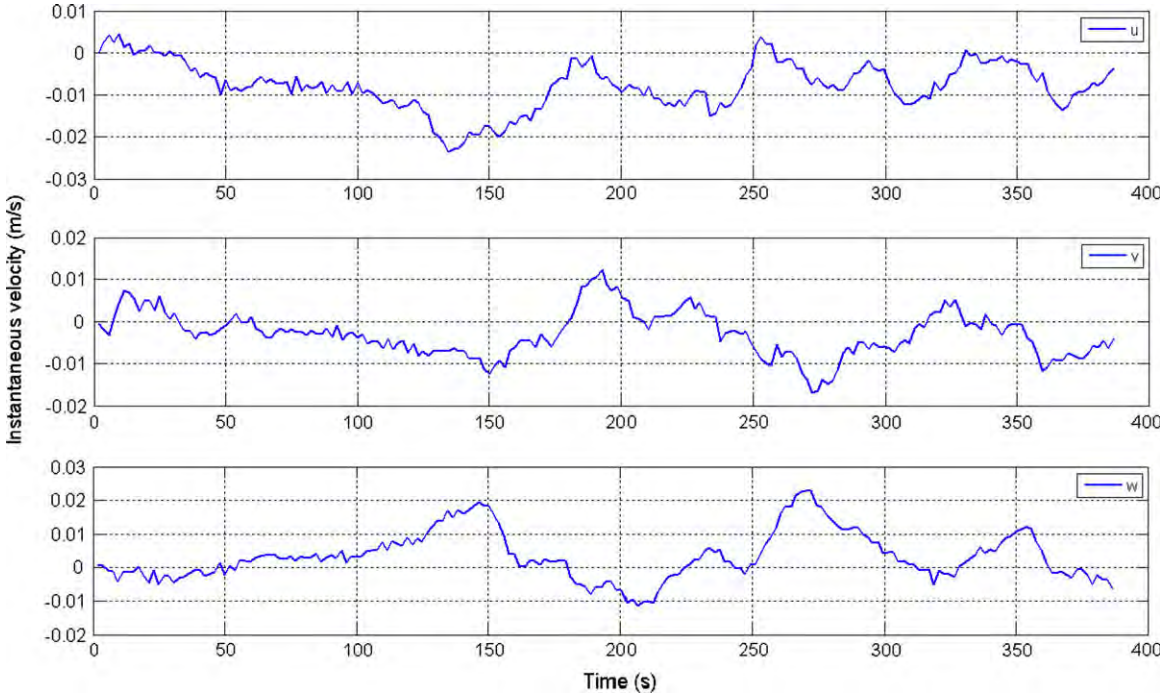

Fig. 6. Time series of instantaneous velocity at a point (1.125 m, 1.20 m, 1.125 m) for a finer grid using URANS method with RFG in the DREAM code.

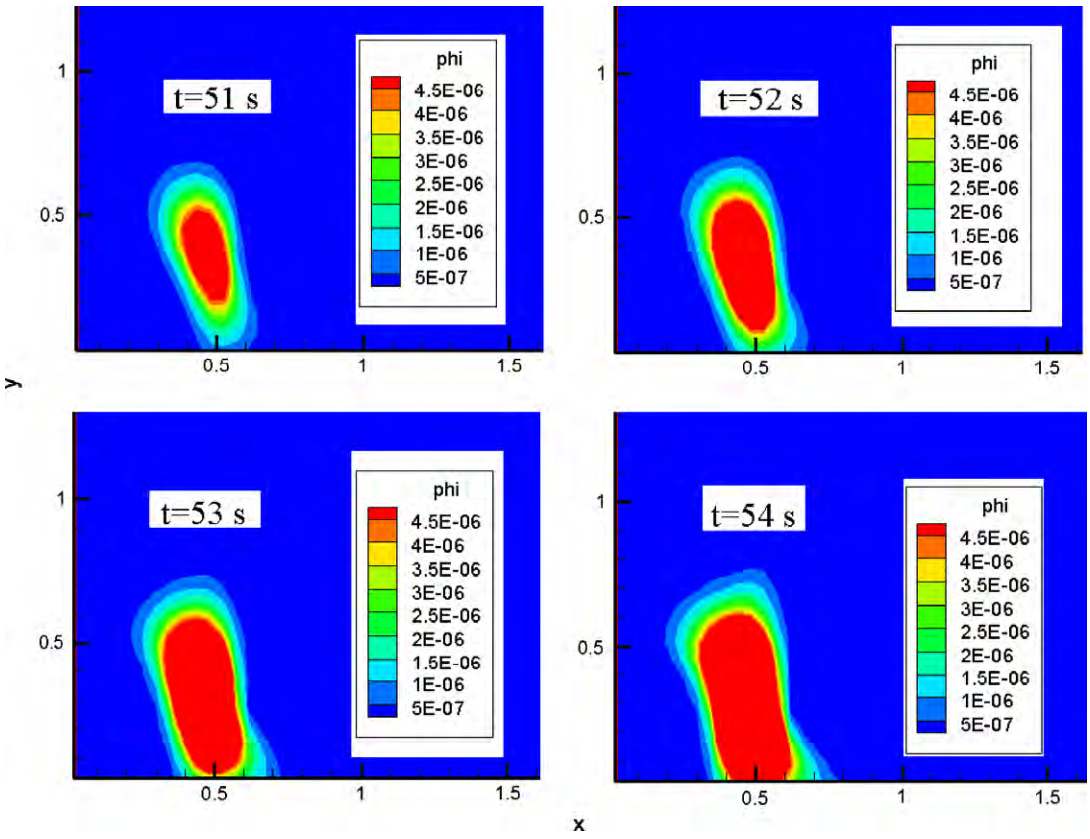

Fig. 7. Contours of instantaneous concentration of particles at four consecutive instants (time interval of 1 s) in the room without considering effects of coughing jet on the dispersion of scalar.

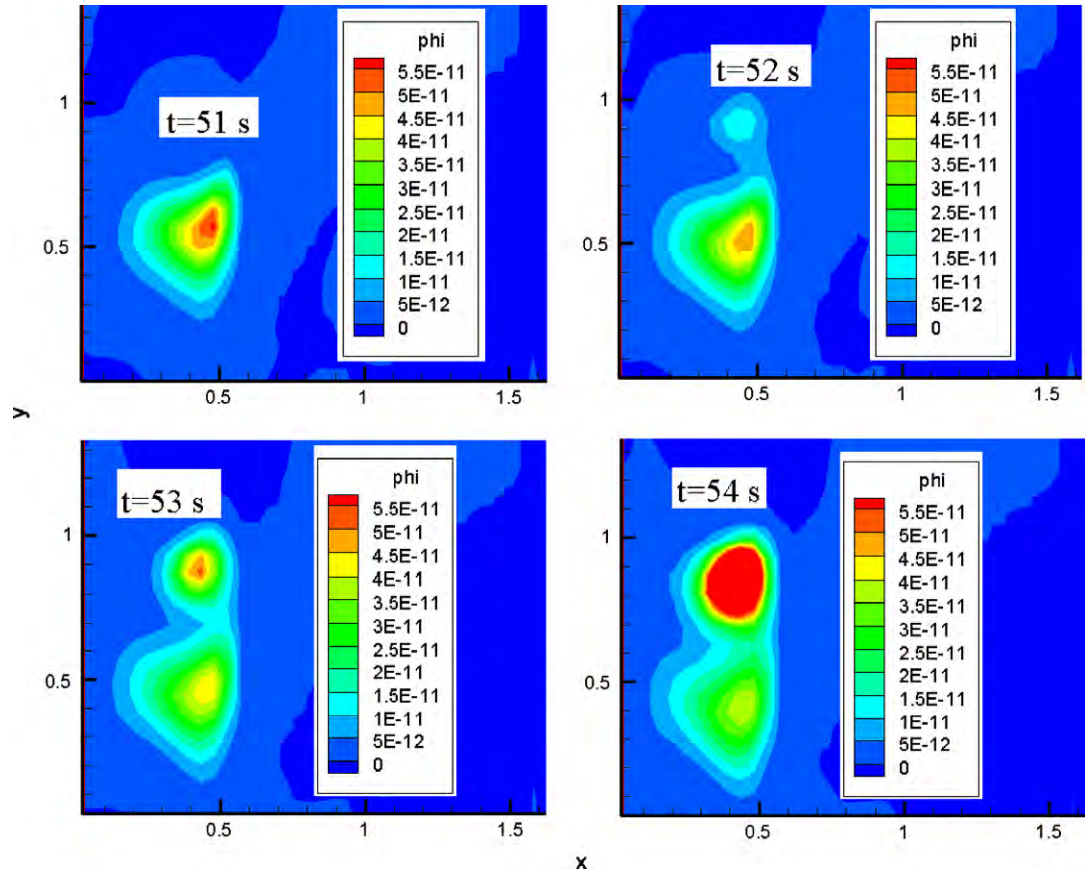

Fig. 8. Contours of instantaneous concentration of scalar, a similar case as in Fig. 7 except that the effect of coughing jet (maximum velocity of 2.5 m s^{-1}) is included.

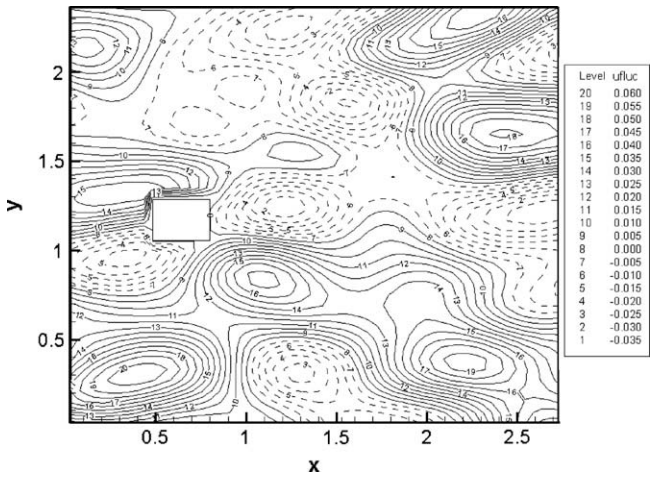

Fig. 9. Contours of small scale u velocity fluctuations (m s^{-1}) at the central vertical cross section for the same ventilation room by using RFG. x and y in meters.

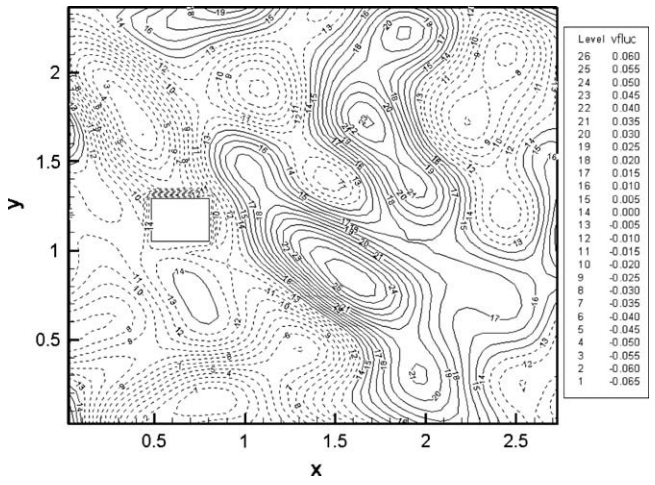

Fig. 10. Contours of small scale v velocity fluctuations (m s^{-1}) at the central vertical cross section for the same ventilation room by using RFG. x and y in meters.

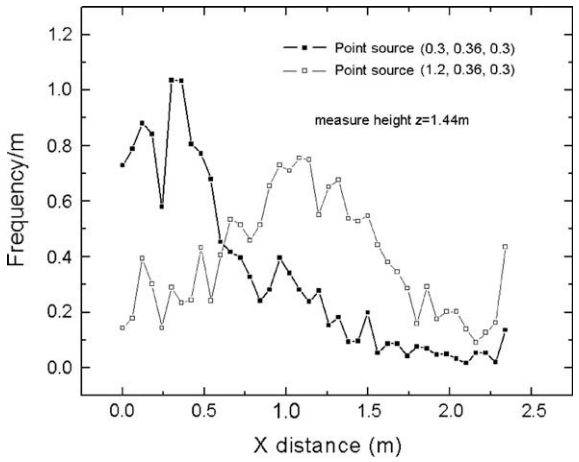

Fig. 11. Probability distribution of aerosol along the horizontal direction at the height z = 1.44 m for two different position of point sources in a ventilated room (without effects from coughing jet).

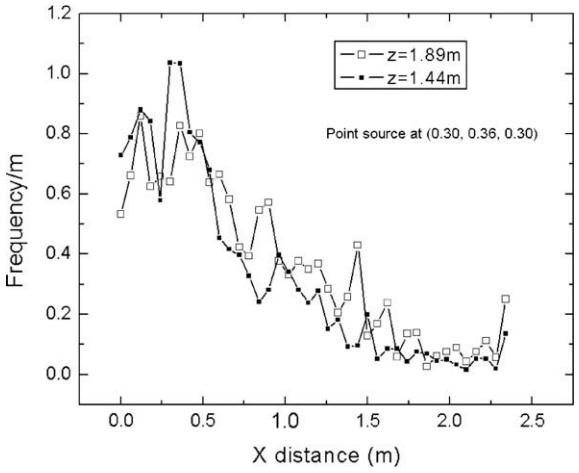

Fig. 12. Probability distribution of aerosol along the horizontal direction for two heights z = 1.44 m and 1.89 m from the same point sources in a ventilated room (without effects from coughing jet).

the mean flow is zero. An special turbulent transport model is required [17]. Instead of using complex specific model, Random flow generation (RFG) technique is applied to reconstruct turbulence while the mean velocity is zero. In addition, second-moments such as Reynolds stresses and co-variances can be easily calculated from RFG.

Figs. 9 and 10 show the instantaneous turbulent u and v velocity fluctuations on a vertical cross section (A–A) where the mean velocity is zero. For the ventilation conditions shown in Fig. 3, the magnitude (turbulent intensity) of the small-scale turbulence is about 5% of the large scale turbulence. The contour lines show complicated coherent structure of turbulence in the room. We again see that the advantage of RFG model is its simplicity and feasibility to generate anisotropic turbulence. For turbulent flow that mean velocity is not zero, a full scale realistic flow field is reconstructed by superimposing the small-scale turbulent fluctuation as shown in Figs. 9 and 10 to the large scale instantaneous velocity calculated from URANS (Figs. 4 and 5).

Given the source location, the LS walk model can predict the transport and dispersion of aerosols, and calculate the probability density function (PDF) or influence area of aerosols in the ventilated room. Two point source positions are chosen, and 50,000 particles have been released at a given point for each run. The statistics of the probability distribution is based on 1000 s of real time simulation. Since it is easy to obtain the time trace of particle concentration at a given sample position [29], the probability distribution in space can be also used to compare to that time trace for quasi steady state turbulent flow based on Taylor's hypothesis.

Figs. 11 and 12 show the probability distribution of aerosol concentration under a small-scale turbulence condition (the mean velocity is zero in the closed room). The risk area of infection is directly reflected from the location of peak of each distribution curve (proportional to location of peak). Fig. 13 shows the effects of point source on the probability distribution of aerosols. The local peak is determined by the position of source. Fig. 12 shows the redistribution of aerosol concentration at different measurement height (1.44 m and 1.89 m in the room) for the same point source. This quantitative comparison shows that more particles could accumulate at the height of 1.44 m than that at z = 1.89 m. Fig. 13 shows the normalized concentration or probability distribution of aerosols, which provides quantitative information of impact area in a statistical sense. There are two issues to be emphasized: first, the distribution of occurrence is only for a limited statistical period (1000 s of real time). Second, a threshold condition is set up for turbulent kinetic energy of aerosol to determine whether it will

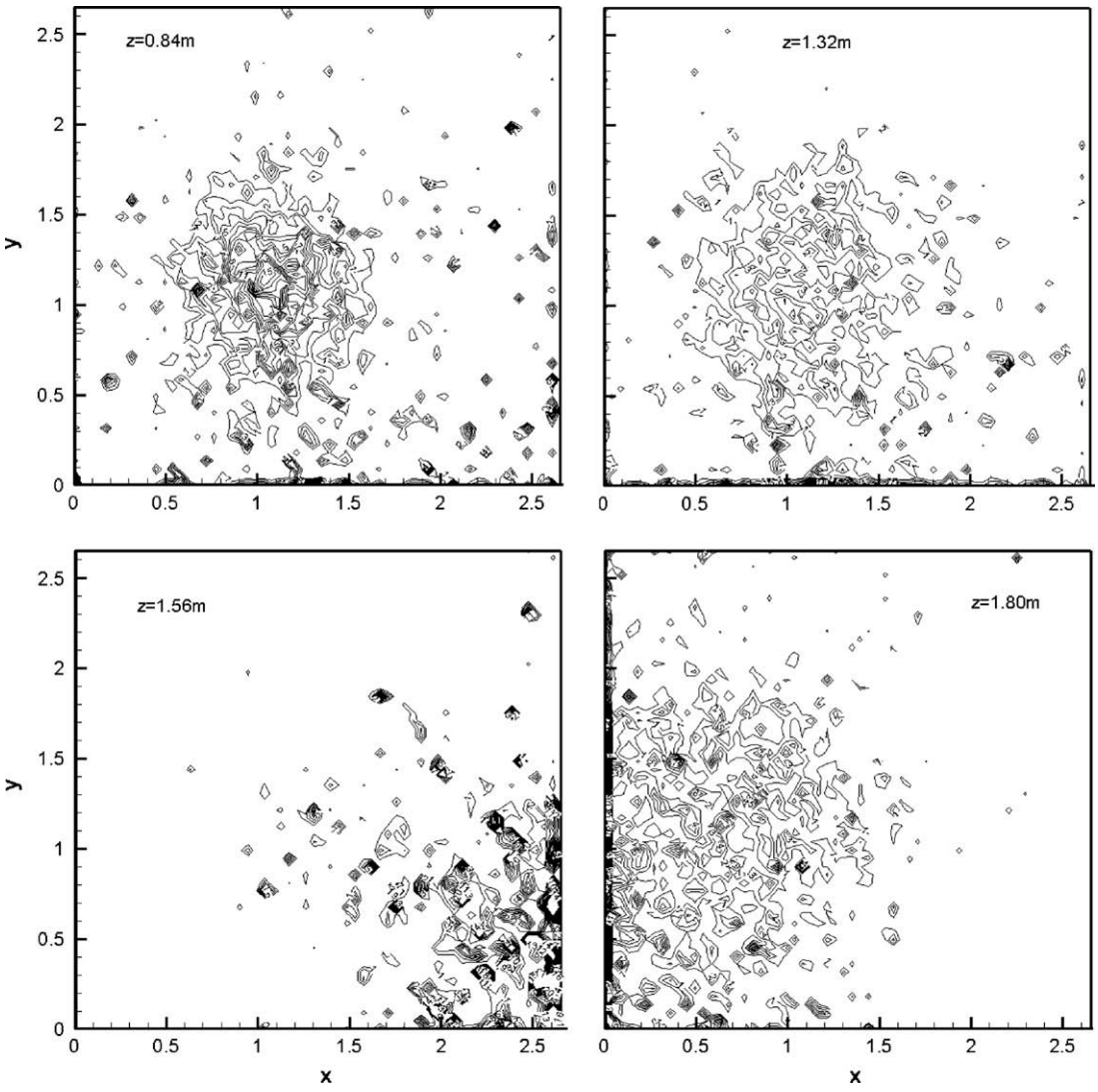

Fig. 13. Normalized concentration of probability distribution of particle at different measurement height levels obtained by combined RFG technique and the LS model.

rebound or not when it gets in contact with floor/ceiling/walls. There will be a small difference in the probability distribution close to the wall if a non-rebounding condition is used. Nevertheless, we can see clearly that the results with probability distribution can provide more quantitative information than that from predicted trajectories of particles as reported by most previously published research work.

4. Conclusions

A numerical tool (i.e. DREAM code) based on unsteady RANS with no turbulence model (URANS) has been developed. The large-scale turbulent flow was directly solved by using URANS in a relative coarse grid system. The random flow generation (RFG) technique was applied to generate the small-scale turbulence based on prescribed turbulent length-scales and time-scales and superimposed to large-scale velocity components. In addition, the RFG can reconstruct the weak turbulent fluctuations where the mean velocity is zero. Otherwise, a special turbulent transport model is required for low-Reynolds number flow inside weaker ventilated rooms. On the other hand, the RFG can be used as a sub-grid scale (SGS) model to large-eddy simulation (LES). The numerical results obtained by URANS + RFG have effectively captured re-circulation zones and turbulent fluctuations and show advantages over RANS models.

Immersed boundary method is successfully implemented in the newly developed code. This technique can be applied with relative easy with a structured Cartesian grid system for complex geometries that are often encountered in bio-fluids and environmental flow problems. Numerical experiments show promising results compared to complicated body-fitted grid system. A typical ventilation system was tested by using immersed boundary method for indoor airflow and dispersion of aerosols. This technique can also be applied to other engineering problems such as porous media problems and other multi-phase flow applications.

A Langrangian stochastic (LS) flight model combined with RFG technique was applied to examine the risk of infection in a typical ventilated room. This model is shown to be feasible for analyzing complicated indoor environment in which turbulence diffusion exhibits significant effect on the transport of aerosol particles. The calculated probability distribution (or normalized concentration) of aerosols (droplet nuclei) in a typical ventilated room showed that the peak of influence area moved away from the coughing source as aerosols propagate with air (the carrier phase). It also shows the effects of entrainment and deposition of aerosols. The probability distribution provides quantitative information to directly assess influence area of virus-laden aerosols due to turbu-

lent diffusion in a closed space. This result is more useful than that shown in random trajectories of particle as widely reported in the literature. This type of numerical results should help us to reexamine indoor environments in healthcare settings and other work places to limit or prevent viral spread.

Acknowledgement

This work is funded by Innovative Management & Technology Services, LLC (IMTS) under Contract No.: IMTS-WVHTC-W-NASA-ED-07-1350-WVU, and by the Grant No.: 1 R01 OH009037-01 from CDC-NIOSH. Its contents are solely the responsibility of the authors and do not necessarily represent the official views of US DHHS/CDC/NIOSH. The authors also want to thank Dr. A. Posada for his repeated reviewing and editing of the manuscript.

References

[1] Badeau Jr Allen E. Analysis of a curved buoyant jet in an enclosure using LES. PhD Dissertation. West Virginia University; 2003.
[2] Beggs CB. The airborne transmission of infection in hospital buildings: fact or fraction? Indoor Built Environ 2003;12:9–18.
[3] Brachman PS. Transmission and principles of control. In: Mandell GL, Douglas RG, Bennett JE, editors. Principles and practice of infectious diseases. New York: Churchill Livingstone; 1990. p. 155–8.
[4] Celik IB, Mao S, Karaismail E. Development of novel CFD tools for bioengineering applications. Final Report No.: MAE-IC08TR01. West Virginia University; 2008.
[5] Chandrasekhar S. Brownian motion, dynamical friction, and stellar dynamics, Rev. Mod Phys 1949;21(3):383–8.
[6] Chen SC, Chang CF, Liao CM. Predictive models of control strategies involved in containing indoor airborne infections. Indoor Air 2006;16:469–81.
[7] Chen Q. Computational fluid dynamics for HVAC: successes and Failures. ASHRAE Trans 1997;103:178–87.
[8] Chung KC. Three-dimensional analysis of airflow and contaminant particle transport in a partitioned enclosure. Build Environ 1999;34:7–17.
[9] Crowe C, Sommerfeld M, Tsuji Y. Multiphase flows with droplets and particles. CRC Press; 1998. 471p.
[10] Durbin PA. Stochastic differential equations and turbulent dispersion. NASA Reference Publication 1103;1983.
[11] Fennelly KP, Davidow AL, Miller SL, Connell N, Ellner J. Airborne infection with *Bacillus anthracis* – from mills to mail. Emerg Infect Dis 2004;10(6):996–1001.
[12] Hinds WC. Aerosol technology. John Wiley & Sons; 1982. 424p.
[13] Hu Gusheng. Towards large eddy simulation of dispersed gas–liquid two-phase turbulent flows. PhD Dissertation. West Virginia University; 2005.
[14] Hu G, Celik I. Eulerian–Lagrangian based large eddy simulation of a partially aerated flat bubble column. Chem Eng Sci 2008;63:253–71.
[15] Kao PH, Yang RJ. Virus diffusion in isolation rooms. J Hosp Infect 2006;62:338–45.
[16] Kraichnan R. Diffusion by random velocity field. Phys Fluid 1970;11:43.
[17] Launder BE, Spalding DB. The numerical computation of turbulent flows. Comp Meth Appl Mech Eng 1974;3:269–89.
[18] Li A, Ahmadi G, Bayer R, Geynes M. Aerosol particle deposition in an obstructed turbulent duct flow. J Aerosol Sci 1994;25(1):91–112.
[19] Li Y, Huang X, Yu ITS, Wong TW, Qian H. Role of air distribution in SARS transmission during the largest nosocomial outbreak in Hong Kong. Indoor Air 2004;15:83–95.
[20] Mao S, Redrow J, Celik IB. Modeling of bio-aerosol transport and dispersion in ventilation room. In: The proceeding of options for the control of influenza VI, Toronto, Ontario, Canada; 2007 [Paper No. P1103].
[21] Morawska L. Droplet fate in indoor environments, or can we prevent the spread of infection? Indoor Air 2006;16:335–47.
[22] Nardell EA, Keegan J, Cheney SA, Etkind SC. Airborne infection: theoretical limits of protection achievable by building ventilation. Am Rev Respir Dis 1991;144:302–6.
[23] Nicas M, Sun G. An integrated model of infection risk in a health-care environment. Risk Anal. 2006;26(4):1085–96.
[24] Nicas M, Nazaroff WW, Hubbard A. Toward understanding the risk of secondary airborne infection: emission of respirable pathogens. J Occup Environ Hyg 2005;2(3):145–54.
[25] Patankar SV. Numerical heat transfer and fluid flow. Hemisphere Publishing Co.; 1980. 197p.
[26] Peskin C. Flow patterns around heart valves: a numerical method. J Comput Phys 1972;10:252–71.
[27] Redrow J, Mao S, Celik I, Posada A, Feng Z. Evaporation and dispersion of airborne biological droplets in confined space. J Aerosol Sci 2010, submitted for publication.
[28] Riley RL. Airborne infection. Am J Med 1974;57:466–75.
[29] Richmond-Bryant J, Eisner AD, Brixey LA, Wiener RW. Transport of airborne particles within a room. Indoor Air 2006;16:48–55.
[30] Rudnick SN, Milton DK. Risk of indoor airborne infection transmission estimated from carbon dioxide concentration. Indoor Air 2003;13:237–45.
[31] Shih Y-C, Chiu C-C, Wang O. Dynamic airflow simulation within an isolation room. Build Environ 2007;42:3194–209.
[32] Smirnov A, Celik I, Shi S. LES of bubble dynamics in wake flows. Comp Fluids 2005;34:351–73.
[33] Smirnov A, Shi S, Celik I. Random flow generation technique for large-eddy simulations and particle-dynamics modeling. ASME J Fluids Eng 2001;123:359–71.
[34] Su M, Chen Q, Chiang CM. Comparison of different subgrid-scale models of large eddy simulation for indoor airflow modeling. ASME J Fluids Eng 2001;123:629–39.
[35] Sun W, Ji Jie, Li Y, Xie X. Dispersion and settling characteristics of evaporating droplets in ventilated room. Build Environ 2007;42:1011–7.
[36] Tellier R. Review of aerosol transmission of Influenza A virus. Emerg Infect Dis 2006;12(11):1657–62.
[37] Tennekes H, Lumley JL. A first course in turbulence. The MIT Press; 1972. ** (Chapter 1).
[38] Tian ZF, Tu JY, Yeoh GH, Yuen RKK. Numerical studies of indoor airflow and particle dispersion by large eddy simulation. Build Environ 2007;42:3483–92.
[39] Wells WF. Airborne contagion and air hygiene. Cambridge: Harvard University Press; 1955.
[40] Xie X, Li Y, Chwang ATY, Ho PL, Seto WH. How far droplets can move in indoor environments – revisiting the wells evaporation – falling curve. Indoor Air 2007;17:211–25.
[41] Yang S, Lee GWM, Chen CM, Wu CC, Yu KP. The size and concentration of droplets generated by coughing in human subjects. J Aerosol Med 2007;20(4):484–94.